Adsorption of natural surfactants present in sea waters at surfaces of minerals: contact angle measurements*

Adriana Mazurek[1]
Stanisław J. Pogorzelski[1,*]
Katarzyna Boniewicz-Szmyt[2]

[1] Institute of Experimental Physics,
University of Gdańsk,
Wita Stwosza 57, PL–80–952 Gdańsk, Poland;

e-mail: dokama@ug.edu.pl, fizsp@ug.edu.pl

*corresponding author

[2] Physics Department,
Gdynia Maritime University,
Morska 81–87, PL–81–225 Gdynia, Poland;

e-mail: kbon@am.gdynia.pl

Abstract

The wetting properties of solid mineral samples (by contact angles) in original surfactant-containing sea water (Gulf of Gdańsk, Baltic) were characterised under laboratory conditions on a large set (31 samples) of well-classified stones of diverse hydrophobicity using the sessile drop (ADSA-P approach), captive bubble and inclined plate methods. An experimental relation between the static contact

The complete text of the paper is available at http://www.iopan.gda.pl/oceanologia/

angle θ_{eq} and stone density ρ was obtained in the form $\theta_{eq} = B\rho + C$, where $B = 12.23 \pm 0.92$, $C = -(19.17 \pm 0.77)$, and $r^2 = 0.92$. The histogram of θ_{eq} distribution for polished stone plates exhibited a multimodal feature indicating that the most abundant solid materials (hydrophilic in nature) have contact angles $\theta_{eq} = 7.2$, 10.7, 15.7 and 19.2°, which appear to be applicable to unspecified field stones as well. The contact angle, a pH-dependent quantity, appears to be a sensitive measure of stone grain size, e.g. granite. The captive bubble method gives reproducible results in studies of porous and highly hydrophilic surfaces such as stones and wood.

The authors consider the adsorption of natural sea water surfactants on stone surfaces to be the process responsible for contact angle hysteresis. In the model, an equation was derived for determining the solid surface free energy from the liquid's surface tension γ_{LV}; it also enabled the advancing θ_A and receding θ_R contact angles of this liquid to be calculated. Measurements of contact angle hysteresis $\Delta\theta(= \theta_A - \theta_R)$ with surfactant-containing sea water and distilled water (reference) on the same stone surfaces allowed the film pressure $\Delta\Pi$ (1.22 to 8.80 mJ m^{-2}), solid surface free energy $\Delta\gamma_S$ (-17.03 to -23.61 mJ m^{-2}) and work done by spreading ΔW_S (-1.23 to -11.52 mJ m^{-2}) to be determined. The variability in these parameters is attributed to autophobing, an effect operative on a solid surface covered with an adsorptive layer of surfactants.

The wetting behaviour of solid particles is of great importance in numerous technological processes including froth flotation, demulgation, anti-foaming procedures and the coal industries. It is believed that the approach presented here and the examples of its application to common sea water/solid mineral systems could be successfully adapted to optimise several surfactant-mediated adsorption processes (see below) of practical value in natural water ecology.

1. Introduction

The adsorption of a surfactant at a solid-liquid interface plays an important role in many technological and industrial applications, such as detergency, mineral flotation, corrosion inhibition, dispersion of solids and oil recovery. In particular, sea water bubbles, even after rising only short distances, are often found to be coated with monolayers and multilayers of particulate material (see Figure 3 in Johnson & Wangersky 1987). Stabilisation occurs when microbubbles are covered with a monolayer of particles with non-polar surfaces. Such particulate monolayers have been shown to possess compression characteristics similar to those of insoluble monomolecular monolayers (Hörvolgyi et al. 1999); they have also been found capable of stabilising foams and emulsions (Adamson & Gast 1997). Moreover, stony material and wood species may be incorporated in the natural surfactant film at the air-sea interface. Such a composite surface has particular surface rheological properties dependent on the particle number flux, particle shape and dimension, and the wettability of the solid material in contact with sea water (Lucassen 1992). Hence, the characterisation of

wetting properties of mineral particles (by contact angles) has attracted significant attention. In this context the term 'wetting' is used to express the process of adhesion (the wetting condition when a sessile drop of water comes into contact with a solid surface), penetration (the wetting condition when water penetrates the pores of a solid by capillary action), and spreading (the wetting condition when water flows laterally over a solid surface).

Sea water is a complex mixture of surface-active organic matter of largely undetermined makeup and concentration, although significant enrichment of many specific classes of compounds has been demonstrated (Hunter & Liss 1992). Contact angle (CA) measurement is a simple tool for quantifying the wettability and the solid surface energy of different materials in contact with pure and surfactant-containing sea water.

This paper examines the adsorption of natural surfactant sea water on stone surfaces as the process responsible for contact angle hysteresis. The surfactant effect on solid/sea water spreading is attributed to autophobing (Ulman 1991) and can be quantified in terms of film pressure, solid surface free energy and the work done by spreading. The work done by spreading is a thermodynamic quantity relating wettability to the mechanical strength of adhesion. It enables the competition between solid-liquid adhesions with different liquids to be characterised (Rodrigues-Valverde et al. 2002, Chibowski 2003). In this paper hysteresis is considered to be due to the surface organic film left behind the drop retreating from its contact line. In consequence, an equation relating advancing and receding contact angles to the total surface free energy of the solid is proposed. In the model, an equation was derived to determine the solid surface free energy from the liquid surface tension γ_{LV}, and the advancing θ_A and receding θ_R contact angles of this liquid (Chibowski 2003).

There are several commonly applied approaches for determining the solid surface free energy and its components from contact angle measurements: the Zisman approach, and also the equation of state, harmonic mean equation, geometric mean equation and acid-base approaches, which Gindl et al. (2001) compared using wood as reference material.

The acid-base (three-liquid method) approach delivers the most detailed information about the surface chemistry in that it gives values for the acidic and basic components in addition to the polar and dispersive components of surface free energy, which is especially valuable with a heterogeneous material. In the present work, however, the contact angle hysteresis (CAH) approach was adopted, relating as it does the total apparent surface free energy of a solid to the surface tension of a sample liquid and its contact angle (CA) hysteresis. Using this formalism, the apparent surface

free energy of a solid and its dispersive component (see eqs. (21)–(22) in Chibowski 2003) can be calculated from the contact angles of only one sample liquid. The equations are based on the assumption that a film of a liquid is left behind a retreating drop. But here no assumption about the film structure is needed. The details and the justification of the CAH approach, as well as a comparison with the results obtained using the acid-base approach of Van Oss et al. (1988) (formulated in the late 1980s with further modifications), which were in very good agreement, are given elsewhere (Radelczuk et al. 2002).

Recently, advancing and receding contact angles were measured on the same sulphur surfaces using two methods – the sessile drop and tilted plate (adapted here for hysteresis calculations) methods (Chibowski & Terpilowski 2008). The tilted plate method (simpler to operate) appears to have some advantages over the sessile drop method: in the former there is no interference with the settled drop (removal of a volume) when the receding contact angle is measured. Experiments have shown that both methods can be applied to contact angle hysteresis measurements because they yield practically the same values of the apparent surface free energy (Chibowski & Terpilowski 2008).

The main difficulty with measuring contact angles on porous structures is capillary action, which yields non-reproducible and meaningless data. Axisymmetric drop shape analysis-profile (ADSA-P) is the most suitable technique for determining contact angles from sessile drops and captive bubbles. It was developed for studies of non-ideal and/or highly hydrophilic surfaces such as stones, cell layers, wood and dentine. Moreover, the captive bubble method used here in conjunction with ADSA-P enables the surfaces of fully hydrated stones to be studied, giving reproducible and accurate contact angles (Rodrigues-Valverde et al. 2002).

The contact angle is a common measure of the hydrophobicity of a solid surface. However, the interpretation of the observed contact angle is complicated by many factors, such as the physical and chemical heterogeneity of the system, the smoothness of the surface, and the presence of surfactants, which can all affect the measured value. While the range of contact angles for natural solid particles in sea water is not known, advancing contact angles for various other substances have been reported (Adamson & Gast 1997); they include Teflon (98°–112°), polyethylene (88° –103°), paraffin wax (110°) and human skin (90°). Whereas natural particles are more typically characterised by contact angles of $< 90°$ (they are of solid hydrophilic material), other factors such as surface roughness or structural and chemical heterogeneity can cause large variability.

Model CA data were obtained on a large set of well-defined stone material (31 samples) and wood species (5 samples) in contact with distilled water (for comparison) and original sea water (collected at Jelitkowo, Gulf of Gdańsk, Baltic Sea, Poland) in order to validate the surfactant-induced effect. For the first time, too, a contact angle dataset was collected for unspecified field stones (50 samples) required as an input parameter in further oceanographic studies of natural physical systems with the composite solid particle-incorporated interfaces come across in the sea.

The atmospheric mineral dust investigated was composed mainly of quartz, anhydrite, plagioclase, haematite, gehlenite and calcite. Lime, alkali feldspars, bassanite, gypsum, mica and unburnt lignite were also found in minor or trace amounts (Sakorafa et al. 1996). A large proportion of the suspended particulate matter in estuarine and coastal waters exists in the form of amorphous aggregates, or flocs, which are composed of inorganic material particles and biogenic debris as well as organic matter, such as cells, cellular exudates and humic material (Gentien et al. 1995).

It is believed that the approach presented here and the examples of its application to common sea water/solid mineral systems could be successfully adapted to optimise several surfactant-mediated adsorption processes (see below) of practical value in natural water ecology (Paria & Khilar 2004):

1. Mineral/particulate flotation.
   At present, mineral flotation is industrially the most important example of a particulate flotation process. Particulates successfully removed from suspension by flotation include bacterial spores, algae, clays and colloidal precipitates.

2. Surfactant-enhanced carbon regeneration.
   Adsorption beds containing activated carbon are commonly used to remove organic pollutants from waste waters. A concentrated surfactant solution is passed through the adsorber containing the spent carbon, and the adsorbate is desorbed and solubilised in the micelles.

3. Herbicide dispersions.
   Nowadays, the success of weed control technology in agriculture can be attributed to the development and effective use of organic herbicides, followed by the use of herbicide adjuvants, in particular, surfactants. These are primarily used in aqueous dispersions, where they reduce surface tension and consequently increase the spreading and wetting of the weed surface.

4. De-inking from paper and plastic film.
   Flotation de-inking is the most important method in paper recycling. In this process, the surfactants are necessary to remove ink from the

fibre during the pulping step and to cause the pigment particles to be separated from the paper fibres by flotation.

5. Filtration of ultra-fine particles.
   The removal of particulate contaminants is very important in water reclamation facilities, water treatment processes, and in the microelectronics and pharmaceutical industries. Adsorption of an appropriate surfactant on the filter surface can lower the energy barrier between the particles and the filter surface, thereby increasing the deposition of small particles on the filter surface.

6. Stability of a particulate suspension.
   The stability of particulate and colloidal slurries is an important phenomenon in many industrial processes such as the manufacture of paints, printing inks and pharmaceuticals. The settling of particles that successfully form a suspension is often caused by the shielding of surface charges on the particles; this results in coagulation and subsequent settling. It has been found that the addition of conventional stabilising agents (e.g. ionic surfactants, polymers) enhance particle stability.

7. Detergency.
   Surfactant molecules are adsorbed on both soil and fabric surface in the process of detergency. The adsorption of surfactants plays a dual role in the removal of soil. They reduce the attraction between soil and fabric by attaching themselves to both. In this way surfactants not only loosen the soil from the fabric but at the same time deflocculate the particles, breaking these up into colloidal particles and stabilising their aqueous dispersion. Soil forming a fine and stable dispersion in the wash liquor is much less likely to attach itself to the fabric during the remaining wash cycle than soil present as a coarse and unstable dispersion.

It is expected that the present studies will provide a good starting point for the characterisation of structures covering the sea bed.

2. Theoretical background

The classic formulation of the force balance on the contact line, known as the Young-Dupré equation (eq. (1)), predicts the contact angle θ in terms of interfacial free energies of the three interfaces of the system (Adamson & Gast 1997):

$$\gamma_{SV} - \gamma_{SL} = \gamma_{LV} \cos\theta, \tag{1}$$

where γ_{SV}, γ_{SL}, and γ_{LV} are the surface free energies between solid/air,

solid/water and water/air respectively, and θ is the contact angle (see Figure 1a in Li 1996). The captive bubble and sessile drop methods, used for determining the contact angle, are based on the same theoretical information (eq. (1)). An air bubble is injected beneath a surface immersed in a liquid and is transported to the solid surface as a result of the buoyant force. The contact angle displayed coincides with the supplementary contact angle corresponding to an 'inverted' sessile drop, as depicted in Figure 1b (Amirfazli & Neumann 2004). The surface is assumed to be totally hydrated, so that there exists between the solid and the bubble a thin layer of water with the air/liquid interface intact. The effect of drop (bubble) size and the correlation between the contact angles of sessile drops and captive bubbles on different surfaces has also been addressed (Drelich et al. 1996). The modification of the surface tension of any of these interfaces changes the wetting characteristics of the solid. The most common interfaces at which surfactants are thought to govern surface free energy are those between air and water, and between a solid and water.
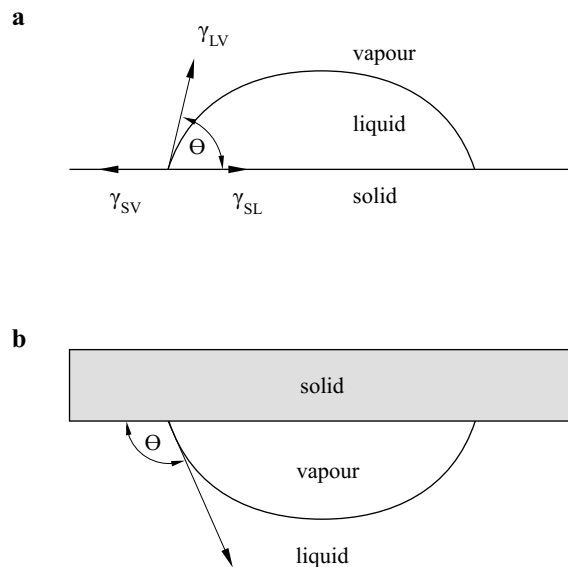
Figure 1. (a) Illustration of an equilibrium sessile drop system (Li 1996); (b) vapour bubble submerged in the liquid phase and in contact with a solid surface; θ represents the contact angle (Amirfazli & Neumann 2004)

The validity of Young's equation requires that the solid surface should be chemically homogeneous, smooth, flat, non-porous, insoluble, non-deformable and of a non-reactive quality (Tavana et al. 2004). On the basis of Young's equation one would expect there to be only one value of

the wetting contact angle θ_{eq} for a particular solid/liquid drop/gas system. However, in practical systems, at least two different contact angles can be measured on the same solid surface and for the same liquid; they are termed the advancing and receding contact angles.

Since nearly all surfaces are heterogeneous and rough to an appreciable extent, a liquid in contact with such surfaces exhibits more than one contact angle. Two of these contact angles are of practical significance for the characterisation of solids. The contact angle measured for a liquid tending to advance is called the 'advancing contact angle' θ_A; it is larger than the contact angle measured for a liquid tending to recede, which is known as the 'receding contact angle' θ_R. The contact angle hysteresis is the difference between the advancing and receding contact angles ($\Delta\theta = \theta_A - \theta_R$), and is no greater than a few degrees for a well-prepared (polished and clean) and stable solid surface.

Some authors attributed contact angle hysteresis to the roughness and heterogeneity of surfaces, as well as to metastable surface energy states (Erbil et al. 1999). Others found that the hysteresis decreases with increasing molecular volume of the liquid on monolayers. More recently, contact angle hysteresis was found to be related to molecular mobility and surface packing, liquid penetration and surface swelling (as reviewed by Lam et al. 2002). The spreading parameter S is the difference between the free energy of the uncovered and the liquid-covered regions of the substrate and is given by:

$$S = \gamma_{SV} - \gamma_{SL} - \gamma_{LV}. \tag{2}$$

When S is positive, the solid-vapour interface has a higher free energy than the liquid-covered region, so the surfactant solution will spontaneously wet the substrate to a final contact angle of zero, a situation known as spreading. Conversely, when S is negative, a non-zero contact angle results and the solution is said to partially wet the surface (De Gennes 1985). Therefore, the wetting behaviour of a surfactant solution depends on the relative surface tension of the solution and the surface energy of the substrate.

Contact angle hysteresis is noticeable on all film-modified surfaces. Because of the film's presence, the solid surface free energy γ_{SF} is changed and can be expressed by the following (Chibowski 2003):

$$\gamma_{SF} = \gamma_{SV} + \Pi, \tag{3}$$

where Π, the film pressure:

$$\Pi = \gamma_{LV}(\cos\theta_R - \cos\theta_A). \tag{4}$$

Note that since the liquid does not spread spontaneously (so-called contact-angle liquid) over the solid surface, the film pressure must be

positive, i.e. the film increases the apparent free energy of the solid surface in the vicinity of the retreating droplet. If a liquid does not form any definite contact angle, i.e. its surface tension is less than the free energy of the solid surface, then the film pressure is negative and in eq. (3) it will take a negative sign, the more so in real systems, where a certain amount of liquid from a drop will always remain on the solid surface, forming a film. If this model is a correct representation of reality, the total surface free energy of a solid $\gamma_{SV}(\equiv \gamma_{SF})$ can be calculated from three measurable parameters, i.e. the sample liquid surface tension and its advancing and receding contact angles measured on the investigated solid surface (Chibowski 2003):

$$\gamma_{SV} = \Pi(1 + \cos\theta_A)^2/[(1 + \cos\theta_R)^2 - (1 + \cos\theta_A)^2]. \tag{5}$$

Equation (5) was derived on the assumption that a residual film of the liquid remains behind the retreating drop. But no such assumption about the film structure is needed. So far, hysteresis has been considered mostly in the context of solid surfaces roughness and/or its chemical heterogeneity.

Film-attributed contact angle hysteresis should be related to the work done by a liquid spreading on a solid surface W_S, which can be easily calculated from the work of adhesion W_a and the work of cohesion W_c:

$$W_S = W_a - W_c, \tag{6}$$

where $W_a = \gamma_{LV}(1 + \cos\theta_A)$ and $W_c = 2\gamma_{LV}$ (Adamson & Gast 1997).

3. Material and methods

3.1. Material

The distilled water used for the contact angle measurements, obtained from a water deionisation apparatus (Millipore, conductivity 0.05 μS cm^{-1}), had a pH of 5.8 ± 0.1 and a surface tension of 72.5 ± 0.2 mJ m^{-2} at 20°C. The pH of the aqueous phase was adjusted to 4–12 by the addition of 0.1 M HCl or NaOH. The surface tension, accurate to 0.1 mJ m^{-2}, was monitored by the Wilhelmy plate method (a 5-cm wide filter paper plate attached to a force sensor (GM2 + UL5, Scaime, France)). Sea water (pH 8.2 ± 0.1; $\gamma_{LV} = 60.2 \pm 0.1$ mJ m^{-2} at 20°C) was collected at Jelitkowo on the Gulf of Gdańsk, Baltic Sea, on 15 November 2006. A large set of stones (31 samples) of well-documented origin and diverse hydrophobicity was used as the model solid substrate. The density of the minerals was determined volumetrically using regularly-shaped pieces of sample materials and an electronic balance. The densities were accurate to within 0.01 g cm^{-3}, as set out in Table 1 (see page 389), and agreed very well with the data provided by the supplier of the materials.

The roughness and heterogeneity of a solid sample can easily conceal interfacial information. In the preparation of high quality surfaces, therefore, it is essential to ensure that the measurements reflect the true interaction between the solid and the liquid. For this reason the stones were cut with a slicer and attached to microscope slides with an inert resin to produce smooth sheets of arbitrary thickness. The samples of wood (oak, beech, birch, pine, spruce) were used as received.

The stone sheets were kept immersed in water and the wood samples were kept covered before use to prevent dust particles from accumulating on their surfaces. Before each measurement, the samples were liberally sprinkled with water and then dried in air. Being natural materials, stones and wood have substantial variations in their structures and chemical compositions, which are reflected by a significant scatter of results for any measured property. This difficulty can be minimised by taking a large number of replicate experimental results (10–15 for each sample here).

3.2. Methods

3.2.1. Sessile drop method

Axisymmetric drop shape analysis-profile (ADSA-P) is used to determine liquid-fluid interfacial tensions and contact angles from sessile as well as pendant drops. This technique was developed to measure contact angles on non-ideal and/or highly hydrophilic surfaces such as cell layers, stones, wood and dentine. The strategy employed is to fit the meridian of an experimental drop profile to the theoretical drop profile according to the Young-Laplace equation, using the surface (interfacial) tension as one of the adjustable parameters (Rodrigues-Valverde 2002). The ADSA-P set-up is briefly described as follows. A CCD monochrome camera with a resolution of 752 x 582 pixels and a horizontally oriented 15x magnifying microscope were used to acquire sessile drop(or bubbles) images. These images were stored in a PC-class computer and processed by a frame grabber. The drop was illuminated from behind with a white-light source shining through a heavily frosted diffuser. This minimised the heat input to the drop and provided a uniformly bright background of white light, which resulted in high contrast images. The temperature of the chamber housing the cell was controlled using a circuit of water at the desired temperature (T = $22 \pm 0.2°$C). The sample cell was placed on an adjustable support, allowing the surface to reach exactly the horizontal position. For non-circular drops, e.g. oval, or those with irregular three-phase contact lines, an equivalent maximum diameter must be used to find the average contact angle. The equivalent maximum diameter is defined as the maximum diameter corresponding to an axisymmetric drop with the same volume as the actual drop. For this

reason, the mean drop diameter $< d_{max} >$ and the mean drop quadratic diameter $< d^2{}_{max} >^{1/2}$ are defined from the perimeter L and the cap area A by:

$$< d_{max} > \equiv L/\pi \qquad < d^2{}_{max} >^{1/2} \equiv 2(A/\pi)^{1/2}. \qquad (7)$$

Furthermore, the volume of a spherical cap V of radius R and the surface area of a liquid-vapour interface A are related as follows (Gokhale et al. 2005):

$$V = \pi R^3/3(1 - \cos\theta)^2(2 + \cos\theta) \qquad A = 2\pi R^2(1 - \cos\theta). \qquad (8)$$

3.2.2. Captive bubble method

The captive bubble method is used as an alternative method (Grundke et al. 1996, Prokop et al. 1998). A captive bubble arrangement in conjunction with ADSA-P was used to quantify the wettability of several types of stones and wood samples in contact with pure and sea water. The sample was placed in a rectangular glass cell, which was then filled with water. Air bubbles of varying size (radius from 1 to 7 mm, as recommended in Drelich et al. 1996) were generated at the tip of a U-shaped needle using a syringe (with an accuracy of 0.1 mm^3) and released from the needle. The released bubbles were captured at the solid surface as a result of buoyant transport and attachment. After the air bubbles had become attached to the solid surface, the contact angle was measured with ADSA-P. Five captive bubbles were formed on each sample and the picture-derived shape parameters averaged.

3.2.3. Inclined plate method

Contact angle hysteresis and drop shape can be studied with a tiltable plane (Extrand & Kumagi 1995). For a drop on an inclined plane (see Figure 2), the front edge of the drop creeps forward while the rear edge remains fixed. The contact angle of the advancing edge θ_A increases and the angle of the receding edge θ_R decreases. If the retentive force exceeds a critical value at a certain angle of the plane inclination, then the drop as a whole begins to move; this then gives the correct values of θ_A and θ_R for the studied system.

After the solid material sample had been attached to the plane, a liquid drop was deposited on the substrate using a variable-volume pipette, and then the plane was slowly tilted. When the drop began to move, the critical advancing and receding contact angles θ_A and θ_R were measured from side-view images. These side-view pictures of the drops were taken with a CCD camera, camera lens, frame grabber and PC-class computer for drop
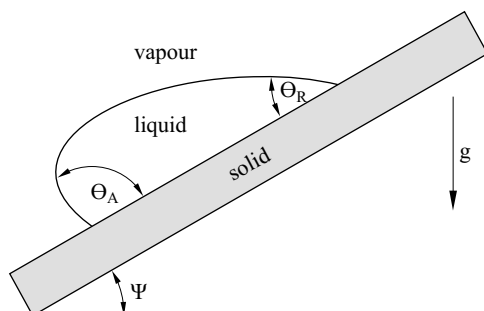
Figure 2. Schematic view of a liquid drop on a tilted solid plane, where Ψ is the angle of tilt, and θ_A and θ_R are the advancing and receding angles respectively (Extrand & Kumagi 1995)

shape image processing. Magnification was $\sim 15x$. The unperturbed (plane inclination angle $\Psi = 0$) drop-sample contact diameter 2R ranged from 5 to 10 mm. All measurements were done at room temperature ($22 \pm 1°C$). Contact angles were accurate to within $0.1°$ but the repeatability of each measurement was approximately $\pm 1°$.

4. Results and discussion

Mean values of static contact angles θ_{eq}, its hysteresis θ_A, θ_R, $\Delta\theta$, and other parameters important for quantifying spreading, e.g. film pressure Π, solid surface free energy γ_s, and the work done by spreading W_S, are listed in Table 1. They were obtained by the sessile drop (s), captive bubble (c) and inclined plate (i) methods on a set of well-specified solid stones with diverse surface properties, in contact with distilled (s) and sea (sm) water. The standard deviation of the θ determination was within 1.5 degrees. The θ_{eq} values obtained by the sessile drop and captive bubble methods did not differ by more than 1–2 degrees. The captive bubble method in conjunction with the ADSA-P technique allowed reproducible measurements of contact angles on porous stones to be obtained.

When experiments are performed on surfaces such as stone and wood, the signatures of the acquired images make it extremely difficult to distinguish exactly where the sessile drop edge is (see Rodrigues-Valverde et al. 2002). Low contact angles (compare 25 to 31 in Table 1) demonstrate the hydrophilic properties of such a surface. Similarly, the low values of θ_{eq} presented in Figures 6 and 7 in Rodrigues-Valverde et al. (2002) for silicate and calcite sheets immersed in water indicate the highly hydrophilic nature of these stones. The charge state of such stones in an aqueous medium is due to the dissociable superficial groups of the mineral (Si_2O or

Table 1. Static contact angles θ_{eq}, contact angle hysteresis $\Delta\theta$, film pressure Π, solid surface free energy γ_{SV}, and work done by spreading W_S, for a stone solid/water surface system at 22°C

No.	Sample material stones (density [g cm^{-3}])	θ_{eq} [°]	θ_A [i] [°]	θ_R [i] [°]	$\Delta\theta$ [°]	Π [mJ m^{-2}]	γ_{SV} [mJ m^{-2}]	W_S [mJ m^{-2}]
1	roof slate (3.36)	24.2^s 23.1^c 39.5^{sm}	36.2 56.8	12.1 22.6	24.1 34.2	12.38 21.18	62.52 38.91	−13.99 −25.51
2	diabase (3.30)	23.5^s 21.6^c 36.7^{sm}	37.6 52.2	9.4 21.3	28.2 30.9	14.08 17.98	61.63 41.39	−15.06 −21.83
3	anhydrite (3.23)	23.0^s 21.4^c 35.1^{sm}	37.8 50.9	8.2 19.4	29.6 31.5	14.47 17.36	61.45 41.96	−15.21 −20.83
4	fluorspar (3.22)	22.4^s 19.6^c 32.3^{sm}	35.7 46.8	9.1 17.9	26.6 28.9	12.71 15.06	62.65 44.01	−13.62 −17.79
5	granite (low grain-sized) (3.22)	21.5^s 19.3^c 31.4^{sm}	34.5 45.5	8.2 17.3	26.3 28.2	12.01 14.31	63.25 44.61	−12.75 −16.86
6	asbestos (3.12)	20.5^s 20.3^c 30.9^{sm}	33.1 44.0	7.9 17.9	25.2 26.1	11.07 13.10	63.93 45.41	−11.76 −15.38
7	basalt (3.05)	20.0^s 19.4^c 30.2^{sm}	31.8 43.3	7.6 17.2	24.2 26.1	10.24 12.83	64.55 45.70	−10.88 −15.35

Table 1. (*continued*)

No.	Sample material stones (density [g cm^{-3}])	θ_{eq} [°]	θ_A [i] [°]	θ_R [i] [°]	$\Delta\theta$ [°]	Π [mJ m^{-2}]	γ_{SV} [mJ m^{-2}]	W_S [mJ m^{-2}]
8	limestone (rocky) (3.03)	19.5^s 18.7^c 29.4^{sm}	29.7 41.7	9.2 17.2	20.5 24.5	8.59 11.76	65.64 46.45	−9.52 −14.28
9	teschenite (3.01)	19.0^s 18.5^c 28.4^{sm}	28.2 40.4	9.0 16.5	19.2 23.9	7.71 11.12	68.72 47.01	−8.60 −13.44
10	syenite (2.97)	18.7^s 18.1^c 27.5^{sm}	27.9 42.8	8.7 12.1	19.2 30.7	7.59 13.76	66.41 45.66	−8.42 −15.01
11	limestone (conglomerate) (3.27)	18.2^c 17.6^c 26.2^{sm}	29.0 38.2	6.9 14.3	22.1 23.9	8.56 10.33	65.84 47.90	−9.09 −12.07
12	anthracite (3.00)	18.0^s 18.4^c 25.8^{sm}	28.1 37.9	8.3 13.8	19.8 24.1	7.78 10.26	66.27 47.97	−8.54 −11.89
13	cobalt (metallic) (2.99)	17.9^s 17.6^c 24.4^{sm}	27.8 36.6	7.9 12.2	19.9 24.4	7.67 9.84	66.36 48.45	−8.36 −11.12
14	melaphyre (2.93)	16.8^s 16.1^c 26.3^{sm}	26.5 40.7	7.1 12.0	19.4 28.7	7.06 12.40	66.95 46.62	−7.61 −13.64

Table 1. (*continued*)

No.	Sample material stones (density [g cm^{-3}])	θ_{eq} [°]	θ_{A}[i] [°]	θ_{R}[i] [°]	$\Delta\theta$ [°]	Π [mJ m^{-2}]	γ_{SV} [mJ m^{-2}]	W_{S} [mJ m^{-2}]
15	marble (2.89)	16.5[s] 15.4[c] 25.9[sm]	24.3 38.8	7.3 13.1	17.0 25.7	5.83 10.97	67.79 47.54	−6.42 −12.44
16	andesite (2.86)	16.0[s] 15.8[c] 24.8[sm]	23.8 35.2	8.1 14.4	15.7 20.8	5.44 8.54	68.05 49.18	−6.16 −10.31
17	mica (2.85)	15.5[s] 16.1[c] 24.1[sm]	22.9 37.1	7.3 11.2	15.6 25.9	5.12 10.34	68.29 48.22	−5.71 −11.41
18	mudstone slate (2.83)	17.2[s] 15.8[c] 23.6[sm]	26.2 35.9	8.3 11.5	17.9 24.4	6.68 9.58	67.04 48.74	−7.44 −10.71
19	quartz (milky) (2.81)	17.0[s] 16.6[c] 26.4[sm]	25.8 38.7	7.9 14.1	17.9 24.6	6.53 10.68	67.19 47.65	−7.22 −12.38
20	diorite (2.79)	16.5[s] 15.8[c] 26.5[sm]	26.1 39.6	7.0 13.4	19.1 26.2	6.85 11.40	67.10 47.19	−7.39 −12.94
21	granite (medium grain-sized) (2.79)	16.4[s] 15.5[c] 24.4[sm]	25.3 36.7	7.2 12.2	18.1 24.5	6.38 9.90	67.43 48.41	−6.95 −11.17

Table 1. (*continued*)

No.	Sample material stones (density [g cm^{-3}])	θ_{eq} [°]	θ_{A} [i] [°]	θ_{R} [i] [°]	$\Delta\theta$ [°]	Π [mJ m^{-2}]	γ_{SV} [mJ m^{-2}]	W_{S} [mJ m^{-2}]
22	phosphorite (2.77)	15.7$^{\text{s}}$ 13.5$^{\text{c}}$ 23.5$^{\text{sm}}$	21.9 34.4	8.3 12.7	13.6 21.7	4.47 8.48	68.74 49.40	−5.23 −9.86
23	quartzite (2.75)	17.5$^{\text{s}}$ 14.7$^{\text{c}}$ 23.2$^{\text{sm}}$	26.0 35.3	8.6 11.1	17.4 24.2	6.52 9.31	67.21 48.96	−7.23 −10.36
24	gabbro (2.75)	16.2$^{\text{s}}$ 14.5$^{\text{c}}$ 24.4$^{\text{sm}}$	23.9 34.9	7.4 13.9	16.5 21.0	5.61 8.49	67.98 49.27	−6.21 −10.14
25	gneiss (2.71)	12.2$^{\text{s}}$ 13.5$^{\text{c}}$ 19.4$^{\text{sm}}$	19.8 29.6	7.1 9.3	12.7 20.3	3.73 6.61	69.43 51.04	−4.28 −7.36
26	sandstone (quartzite kind) (2.70)	14.6$^{\text{s}}$ 12.5$^{\text{c}}$ 17.6$^{\text{sm}}$	21.1 26.9	7.3 8.4	13.8 18.5	4.27 5.49	68.69 51.93	−4.68 −6.10
27	porphyry (2.69)	14.0$^{\text{s}}$ 12.7$^{\text{c}}$ 20.4$^{\text{sm}}$	20.6 27.9	6.2 12.4	14.4 15.5	4.21 5.24	69.11 51.84	−4.36 −6.55
28	granite (large grain-sized) (2.60)	16.9$^{\text{s}}$ 12.6$^{\text{c}}$ 27.2$^{\text{sm}}$	24.7 39.7	8.7 14.8	16.0 24.9	5.79 11.13	67.65 47.24	−6.63 −13.00

Table 1. (*continued*)

No.	Sample material stones (density [g cm^{-3}])	θ_{eq} [°]	$\theta_{A}{}^{i}$ [°]	$\theta_{R}{}^{i}$ [°]	$\Delta\theta$ [°]	Π [mJ m^{-2}]	γ_{SV} [mJ m^{-2}]	W_{S} [mJ m^{-2}]
29	marl (malm) (2.43)	15.7^{s} 14.2^{c} 21.5^{sm}	21.9 31.0	8.1 12.1	13.8 18.9	4.50 6.80	68.64 50.70	−5.23 −8.05
30	limestone (crynoid) (2.41)	13.1^{s} 10.5^{c} 17.5^{sm}	18.2 27.9	7.3 7.1	10.9 20.8	3.04 6.12	69.92 51.60	−3.62 −6.55
31	gypsum (2.17)	7.8^{s} 5.6^{c} 13.3^{sm}	12.4 19.5	3.1 7.0	9.3 12.5	1.58 2.81	71.02 53.99	−1.69 −3.23

Denotations: s – sessile drop method, c – captive bubble method, sm – sessile drop method on sea water (collected at Jelitkowo, Gulf of Gdańsk, Baltic Sea on 15 November 2006), i – determined with the inclined plate method. Values of γ_{LV}, for distilled and sea water were equal to 72.5 ± 0.2 and 60.2 ± 0.2 mJ m^{-2} respectively.

$CaCO_3$); hence the difference between the contact angles can be explained by the different electrostatic interaction between H_2O molecules and those superficial groups. Magnesite ($MgCO_3$) and dolomite [Ca, $Mg(CO_3)_2$] are two salt-type minerals that are also by nature hydrophilic, exhibiting small contact angles ($10.4°$ and $6.6°$ respectively) in distilled water (Gence 2006).

Effects due to roughness and physicochemical heterogeneity can easily conceal interfacial information. If a smooth solid surface gives an angle (i.e. Young angle θ_{eq}) greater than $90°$, the roughness expressed by the roughness ratio (r = apparent surface area of a rough surface/geometric projected area) increases this contact angle further (to the Wenzel apparent angle θ^*), but if it is less than $90°$ (a property of hydrophilic surfaces found in minerals), roughness decreases the angle. This is the interpretation of the Wenzel equation (Wenzel 1936): $\cos\theta^* = r\cos\theta_{eq}$. The difference $\theta^* - \theta_{eq}$ did not exceed $2°$ for well-polished mineral surfaces, which revealed values of r (1.02–1.03) as evidenced by microscopic analyses of the studied surface micromorphology (data not shown).

Even though the roughness of stones is reduced by initial polishing, they are always heterogeneous. The surface of a stone can be modelled as an ideally smooth, heterogeneous surface consisting of two types of vertical strips distributed randomly, the predominant mineral having a low contact angle and the other components exhibiting a high contact angle (Rodrigues-Valverde et al. 2002). The heterogeneity of such a composite model surface does not cause any contact angle hysteresis, because the liquid-air-solid three phase contact line always crosses the same percentage of the two strips; hence there are no fluctuations in the surface free energy of the system as a whole.

The contact angle appears to be a sensitive measure of stone grain size, as found for granite (compare 5, 21 and 28 in Table 1). θ_{eq} values become higher as the grain size of a stone decreases. There is a relation between θ_{eq} and the density of the studied stones ρ, shown in Figure 3, which can be approximated by a linear function of the form $\theta_{eq} = B\rho + C$, where $B = 12.23 \pm 0.92$ and $C = -(19.17 \pm 0.77)$; $r^2 = 0.92$. The density of the studied stones ranged from 1.92 to 3.36 g cm^{-3} (mean $\pm$ SD = 2.66 ± 0.29 g cm^{-3}). It was found that the contact angle for stones increased with their density. A likely explanation for this is that the density affects the Hamaker constant (4×10^{-21} J for silica in water) of the stones (which is proportional to the square of the numerical concentration of solid molecules) and thus to the dispersion contribution to the solid-liquid interfacial tension. When the density increases the solid-liquid interfacial tension does so too; at the same time $\cos\theta_{eq}$ decreases (and θ_{eq} increases).
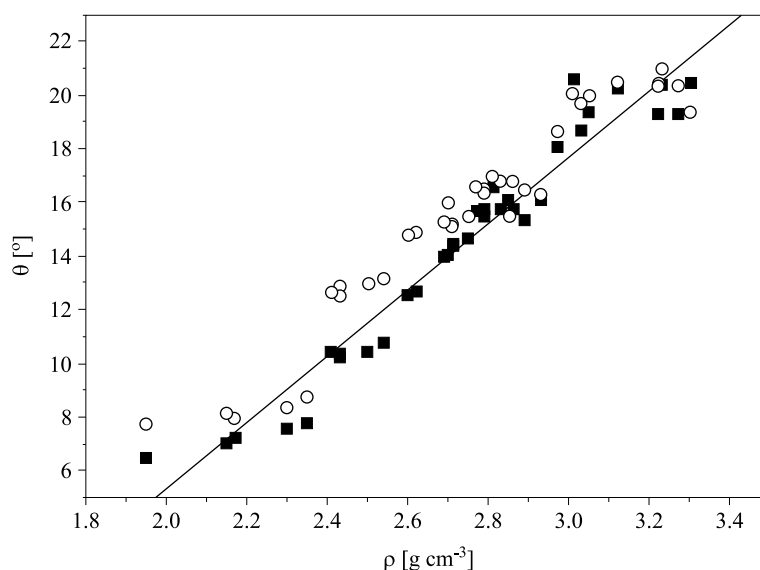
Figure 3. Static contact angle θ_{eq} (obtained by the sessile drop – ○ and captive bubble – ■ methods) versus the density of stone samples. The solid line corresponds to the best-fit linear approximation to the experimental data in the form: $\theta_{eq} = B\rho + C$, where $B = 12.23 \pm 0.92$ and $C = -(19.17 \pm 0.77)$; $r^2 = 0.92$

If this is valid, one expects a linear relationship between density squared and $\cos\theta_{eq}$ (or contact angle squared for a low contact angle, which will probably also fit the data).

Figure 4a shows a histogram of the static contact angle distribution for a solid/water interfacial system at 22°C from measurements performed on a well-specified set of stones. It consists of at least four overlapping distributions exhibiting local maxima at 7.2, 10.7, 15.7 and 19.2°. Since the peak height is related to the relative occurrence of each stone in the set, we are concerned with the four most abundant classes of stones having contact angles varying around the maximum distribution values. A more thorough explanation will require further detailed surface characterisation of the stones using XPS or other surface spectroscopic techniques.

In order to verify whether such a histogram is generally applicable, a large number (50 samples) of unspecified field stones (collected at Gdańsk in May–September 2006) were prepared in the same way as the reference ones and their contact angles determined. Figure 4b presents a histogram of θ_{eq}, which compares data for well-specified stones and unspecified field stones. The general shape of the histogram remained essentially the same,

with four local maxima at 8.2, 12.7, 16.7 and 20.2° shifted by 1–2° to higher contact angles in comparison to Figure 4a.
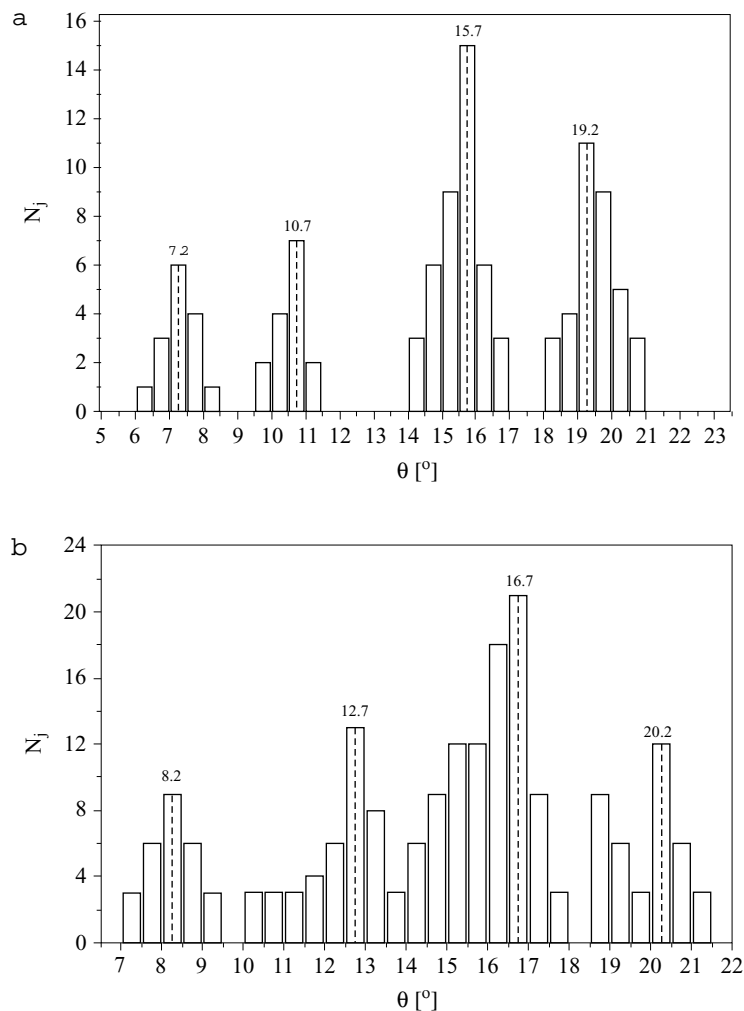
Figure 4. Histogram of the static contact angle θ_{eq} distribution for a stone solid/water surface system at 22°C; (a) – obtained from the data relating to a well-specified set of stones, (b) – derived from the above data supplemented by relating to a large number of unspecified field stones

Values of θ_{eq} for sea water measurements were 5–15° larger than for distilled water. It was found that at the drop edge, a surfactant can adsorb onto the solid-liquid interface, thus giving rise to a surface tension gradient at the liquid-air interface. A hydrophobic barrier builds up at the solid surface as a result of surfactant adsorption in this region. Surfactant

spreading is thought to be halted by a hydrophobic barrier that forms ahead of the drop (Afsar-Siddiqui et al. 2003), which results in an increase in the contact angle.

As the results of the CA hysteresis studies (Table 1) show, the values of θ_A, θ_R and $\Delta\theta$ are several degrees higher for sea water than for distilled water on the same stone sample. Especially the advancing contact angles θ_A in sea water (denoted by 'sm') are larger by as much as 9–20° than in distilled water ('s'), although this difference was less pronounced for most of the hydrophilic stone surfaces (of lower θ_{eq}) studied here. The receding contact angle θ_R for sea water was only a few degrees (3–10°) larger than that of the reference liquid, but again, the deviation was less for more hydrophilic stones (see 17, 18, 22, 29–31 in Table 1). The resulting contact angle hysteresis $\Delta\theta$ attributed to the sample liquid change increased from 9.3 to 34.2° (for the most hydrophobic stone surface – see 1 in Table 1).

In a spreading situation, the contact angle will generally decrease as spreading progresses until a final contact angle is achieved. For complex fluids such as surfactant solutions, the local interfacial energies can be altered in the confined space near the contact line, which controls the contact angle through the Young-Dupré equation (Decker et al. 1999). In autophobing (Ulman 1991), a drop of surfactant solution deposited on a clean surface begins to spread. As the drop spreads, surfactant adsorbs to the surface, lowering the surface energy density so that the solution no longer wets the surface. The edge of the spreading drop then retreats, attaining a final configuration with a high contact angle. The drop resists attempts to force it out again across the surface. A low surface energy 'barrier' has formed parallel to the contact line, which resists the solution's advance. Far from the contact line, the surface energy remains high. Autophobing can be quantified in terms of the corresponding changes in the liquid-solid surface interaction parameters, i.e. the film pressure Π (eq. (4)), total surface free energy γ_{SV} (eq. (5)), and the work of spreading W_S (eq. (6)).

The autophobing of surfactant-containing sea water can be treated as the difference of the above-mentioned spreading parameters referred to distilled water, since there are several other surface phenomena (roughness, sample heterogeneity etc.), which also lead to apparent hysteresis in the stone surfaces studied. The presence of surfactant in sea water causes Π to increase by 20–50% and lowers γ_{SV} by 25–30%, leading to 30–40% more negative values of W_S. Contact angle hysteresis $\Delta\theta$ measurements done on surfactant-containing sea water and distilled water on the same stone surfaces yielded film pressures $\Delta\Pi$ from 1.22 to 8.80 mJ m^{-2}, solid surface free energies $\Delta\gamma_{SV}$ from -17.03 to -23.61 mJ m^{-2}, and work done by

spreading ΔW_S from -1.23 to -11.52 mJ m^{-2}; the variability in these parameters can be attributed to autophobing.

The surface tension of sea water was 60.2 mJ m^{-2} whereas that of the distilled water was 72.5 mJ m^{-2}. When added in small quantities to water, some surfactants can lower its surface tension from ~ 70 to ~ 20 mJ m^{-2} and enable it to wet hydrophobic surfaces without compromising its ability to wet hydrophilic surfaces, thus giving positive values of S (eq. (2)). These surfactants are known as 'superspreaders' (Afsar-Siddiqui et al. 2003). For comparison, the model surfactants used in physical chemistry studies (SDS) lower the surface tension of water to ~ 44, DTAB to ~ 35 and $C_{12}E_m$ to ~ 32 mJ m^{-2}.

It should be mentioned that natural sea water is also a mixture of several electrolytes. Artificial sea water, which mimics original sea water in model studies and is made up as a solution of 0.56 M NaCl, 0.05 M MgSO$_4 \times 7$ H$_2$O and 0.01 M CaCl$_2 \times$ H$_2$O, has pH = 8.5 and salinity $S_a = 35$ PSU. Therefore, the electrolyte effect on the water CA of minerals has to be addressed. For example, the surfaces of feldspars consist of positive and negative sites. The positive sites are mostly Na$^+$ ions in albite and K$^+$ ions in orthoclase, whereas the negative sites are polar silanol groups or non-polar siloxane groups (Karagüzel et al. 2005). The electrostatic charge is mainly a function of pH; raising the pH increases the number of negative species. Conversely, the positive charges increase when the pH is lowered. Table 2 in Karagüzel et al. (2005) shows that the addition of NaCl ($\ll 1$ mol dm^{-3}) leads to a change in CA of less than 3–4 degrees. It should be pointed out that the salinity of Baltic sea waters is evidently lower (5–7 PSU) than that of standard artificial sea water (35 PSU), and that the electrolyte effect may be of secondary importance in the water wettability studies of the model minerals reported here.

Figure 5 shows the static contact angle θ_{eq} as a function of sea water pH at 22°C for stone surfaces such as roof slate, basalt, porphyry and limestone (crynoid). There is a continuous increase in θ_{eq} as pH rises to a maximum at around pH 8.1 (a value close to the sea water pH of 8.4). The maximum is higher for more hydrophobic stone surfaces. Generally, pH influences not only the surface potential, but also the hydrophilicity of the mineral surface (changing structural forces) and the electrokinetic potential of the film-air interface (Churaev & Sobolev 1995). This can also be seen in Figure 2 in Gence (2006), in which an increase in pH caused a slight increase in the contact angle at magnesite and dolomite surfaces in distilled water.

The role played by a surfactant film covering a mineral surface in the liquid-solid contact phenomenon can be appreciated from Figure 3 in Gence (2006), where CA measurements are plotted as a function of system pH
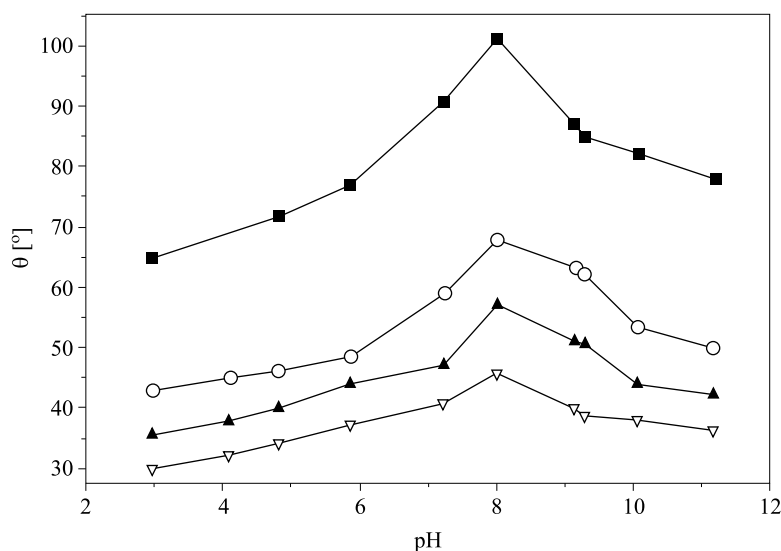
Figure 5. Static contact angle θ_{eq} as a function of sea water pH at 22°C (sea water collected at Jelitkowo, Gulf of Gdańsk, Baltic Sea, on 15 November 2006), for stone surfaces: roof slate – ■, basalt – ○, porphyry – ▲ and limestone (crynoid) – ▽

for magnesite and dolomite treated with various concentrations of sodium oleate. Treatment with this compound enhanced the hydrophobicity of magnesite surfaces, and the maximum contact angle of 79° was obtained at pH 10.2 (av. CA = 41°). In general, the behaviour of surfactants at an interface is determined by a number of forces including electrostatic attraction, covalent bonding, hydrogen bonding and the solvation of various species. The intermolecular forces are of several types: van der Waals, electrostatic, solvation (hydration) and steric (Israelachvili 1992). Steric forces arise when molecules with long chain segments, e.g. surfactants or polymers, are present in the system.

For comparison, the contact angles of sessile water drops on wood surfaces tended to decrease with contact time (see Figure 6). The pronounced decrease in θ within 10 seconds of drop deposition is clearly dependent on the kind of wood and is slower in structurally more compact, higher density species like spruce. This wood sample also exhibited the highest contact angle θ_{eq}. After a sufficiently long time, i.e. 20–30 s, the plot exhibits an asymptotic tendency to reach a constant value, equal to $45.3° \pm 3.7°$ (oak), $26.9° \pm 5.4°$ (beech), $44.5° \pm 1.5°$ (birch), $57.1° \pm 2.0°$ (pine) and $43.1° \pm 3.9°$ (spruce), depending on the porosity of the particular wood surface. This is true since the tendency for a given mass of liquid to spread on a solid surface increases as the contact angle decreases. The
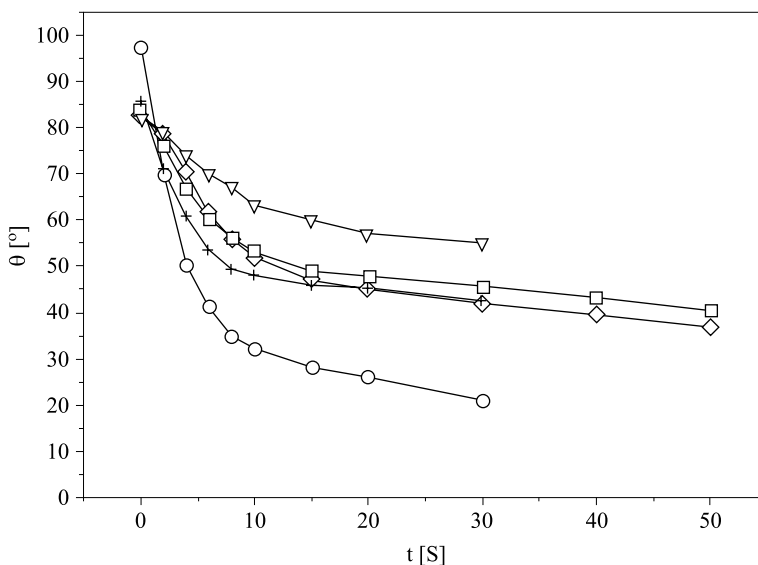
Figure 6. Dynamic contact angle as a function of time elapsed for a seawater-wood sample system at 22°C (sea water collected at Jelitkowo, Gulf of Gdańsk, Baltic Sea, on 15 November 2006). Symbols: wood samples of oak – □, beech – ○, birch – +, pine – ▽, and spruce – ◇

overall lowering of the contact angle of sessile drops with contact time is undoubtedly due to the wetting of the wood. However, particular attention should be paid to effects due to high porosity. Although the drop diameter does not change in time, the drop height and the contact angle decrease. This can be explained by the absorption of the liquid drop through the wood walls. In our case, spreading was faster than possible capillary penetration (Starov et al. 2000).

The contact angle results obtained here on model wood samples were similar to those found in detailed literature surveys (Mohammed-Ziegler et al. 2004). It should be borne in mind, however, that treatment of a wood surface significantly affects its wettability by water. Elevated surface energies have been attributed to the chemical modification of the wood surface by metallic salts with a high surface energy (Tascioglu et al. 2004), whereas mechanical densification of wood significantly decreases its surface energy.

5. Conclusions

The technique most suitable for application on stone surfaces is the captive bubble method in combination with ADSA-P, because the rapid loss of volume due to capillary penetration (porous nature) and rapid spreading

(highly hydrophilic nature) do not permit the sessile drop method to be used. Moreover, the captive bubble method enables the surface of fully hydrated stones to be studied, yielding reproducible and accurate values of CA.

The mineral surfaces studied here displayed largely hydrophilic properties with θ_{eq} in the range $7.8°$–$24.2°$, whereas hydrophobic surfaces were characterised by high contact angles from $40°$ to $110°$. The tendency for static contact angles to increase with stone density can be expressed as a linear dependence in the form $\theta_{\mathrm{eq}} = \mathrm{B}\rho + C$, where $\mathrm{B} = 12.23 \pm 0.92$, $C = -(19.17 \pm 0.77)$; $\mathrm{r}^2 = 0.92$.

The contact angle appears to be a sensitive measure of stone grain structure size, e.g. granite, and is a pH-dependent quantity in the sea water/solid stone surface system.

The histogram of θ_{eq} distribution exhibited a multimodal feature, indicating that the most abundant classes of stones have particular contact angles of 7.2, 10.7, 15.7 and $19.2°$, which appear to be applicable to unspecified field stones as well.

Contact angle measurements in surfactant-containing sea water showed a significant increase, attributable to autophobing, in θ_{eq}, θ_{A}, θ_{R}, and $\Delta\theta$ by several degrees in comparison to the distilled water reference values. Measurements of CA hysteresis enabled the surfactant effect on the solid stone/water surface spreading to be quantified in terms of the film pressure Π (up by 1.22–8.80 mJ m^{-2}), solid surface free energy γ_{SV} (down by 17.03–23.61 mJ m^{-2}), and work done by spreading (changed from $-(1.69$–$15.21)$ to $-(3.23$–$25.51)$ mJ m^{-2}), in comparison with clean water.

Dynamic CA dependences obtained for 5 wood species decreased rapidly within 10 seconds after drop deposition with a gradient $\mathrm{d}\theta/\mathrm{d}t$ dependent on the density of the wood sample and its structure. After a sufficiently long time, asymptotic contact angles were obtained: $45.3° \pm 3.7°$ (oak), $26.9° \pm 5.4°$ (beech), $44.5° \pm 1.5°$ (birch), $57.1° \pm 2.0°$ (pine) and $43.1° \pm 3.9°$ (spruce), related to the porosity of the particular wood surface.

References

Adamson A. W., Gast A. P., 1997, *Physical chemistry of surfaces*, 6th edn., Wiley & Sons, New York, 784 pp.

Afsar-Siddiqui A. B., Luckham P. F., Matar O. K., 2003, *The spreading of surfactant solutions on thin liquid films*, Adv. Colloid Interfac., 106 (1), 183 –236.

Amirfazli A., Neumann A. W., 2004, *Status of the three-phase line tension*, Adv. Colloid Interfac., 110 (3), 121–141.

Chibowski E., 2003, *Surface free energy of a solid from contact angle hysteresis*, Adv. Colloid Interfac., 103 (2), 149–172.

Chibowski E., Terpilowski K., 2008, *Surface free energy of sulfur – Revisited: I. Yellow and orange samples solidified against glass surface*, J. Colloid Interf. Sci., 319 (2), 505–513.

Churaev N. V., Sobolev V. D., 1995, *Prediction of contact angles on the basis of the Frumkin-Derjaguin approach*, Adv. Colloid Interfac., 61, 1–16.

Decker E. L., Frank B., Suo Y., Garoff S., 1999, *Physics of contact angle measurement*, Colloid. Surface. A, 156 (1–3), 177–189.

Drelich J., Miller J. D., Good R. J., 1996, *The effect of drop (bubble) on advancing and receding contact angles for heterogeneous and rough solid surfaces as observed with sessile-drop and captive-bubble techniques*, J. Colloid Interf. Sci., 179 (1), 37–50.

Erbil H. Y., Mc Hale G., Rowan S. M., Newton M. I., 1999, *Determination of the receding contact angle of sessile drops on polymer surfaces by evaporation*, Langmuir, 15 (21), 7378–7385.

Extrand Ch. W., Kumagi Y., 1995, *Liquid drops on an inclined plate: the relation between contact angles, drop shape, and retentive force*, J. Colloid Interf. Sci., 170 (2), 515–521.

Gence N., 2006, *Wetting behavior of magnesite and dolomite surfaces*, Appl. Surf. Sci., 252 (10), 3744–3750.

Gennes de P. G., 1985, *Wetting: statics and dynamics*, Rev. Mod. Phys., 57 (3), 827–834.

Gentien P., Lunven M., Lehaitre M., Dunvent J. L., 1995, *In-situ depth profiling of particle sizes*, Deep-Sea Res. Pt. I, 42 (8), 1297–1312.

Gindl M., Sinn G., Gindl W., Reiterer A., Tschegg S., 2001, *A comparison of different methods to calculate the surface free energy of wood using contact angle measurements*, Colloid. Surface. A, 181 (1), 279–287.

Gokhale S. J., Plawsky J. L., Wayner P. C. Jr., 2005, *Spreading, evaporation, and contact line dynamics of surfactant-laden microdrops*, Langmuir, 21 (18), 8188–8197.

Grundke K., Bogumil T., Werner C., Janke A., Pöschel K., Jacobasch H.-J., 1996, *Liquid-fluid contact angle measurements on hydrophilic cellulosic materials*, Colloid. Surface. A, 116 (1–2), 79–87.

Hörvolgyi Z., Mate M., Daniel A., Szalma J., 1999, *Wetting behaviour of silanized glass microspheres at water-air interfaces: a Wilhelmy film balance study*, Colloid. Surface. A, 156 (1), 501–508.

Hunter K. A., Liss P. S., 1981, *Organic sea surface films*, [in:] *Marine organic chemistry*, E. K. Duursma & R. Dawson (eds), Elsevier, New York, 259–298.

Israelachvili J., 1992, *Intermolecular and surface forces*, 2nd edn., Acad. Press, San Diego, 450 pp.

Johnson B. D., Wangersky P. J., 1987, *Microbubbles: Stabilization by monolayers of adsorbed particles*, J. Geophys. Res., 92 (C13), 14 641–14 647.

Karagüzel C., Can M. F., Sönmez E., Çelik M. S., 2005, *Effect of electrolyte on surface free energy components of feldspar minerals using thin-layer wicking method*, J. Colloid Interf. Sci., 285 (1), 192–200.

Lam C. N. C., Wu R., Li D., Hair M. L., Neumann A. W., 2002, *Study of the advancing and receding contact angles: liquid sorption as a cause of contact angle hysteresis*, Adv. Colloid Interfac., 96 (1), 169–191.

Li D., 1996, *Drop size dependence of contact angles and line tensions of solid-liquid systems*, Colloid. Surface. A, 116 (1–2), 1–23.

Lucassen J., 1992, *Dynamic dilational properties of composite surfaces*, Colloid. Surface., 65 (2–3), 139–149.

Mohammed-Ziegler I., Oszlanczi A., Somfai B., Horvölgyi Z., Paszli I., Holmgren A., Forsling W., 2004, *Surface free energy of natural and surface-modified tropical and European wood species*, J. Adhes. Sci. Technol., 18 (6), 687–713.

Paria S., Khilar K., 2004, *A review on experimental studies of surfactant adsorption at the hydrophilic solid-water interface*, Adv. Colloid Interfac., 110 (3), 75–95.

Prokop R. M., Jyoti A., Eslamian M., Garg A., Michaila M., del Rio O. I., Susnar S. S., Policova Z., Neumann A. W., 1998, *A study of captive bubbles with axisymmetric drop shape analysis*, Colloid. Surface. A, 131 (1), 231–242.

Radelczuk H., Hołysz L., Chibowski E., 2002, *Comparison of the Lifshits-Van der Waals/acid base and contact angle hysteresis approaches to determination of the solid surface free energy*, J. Adhes. Sci. Technol., 16 (12), 1547–1568.

Rodrígues-Valverde M. A., Cabrerizo-Vílches M. A., Rosales-López P., Páez-Duñeas A., Hidalgo-Álvarez R., 2002, *Contact angle measurements on two (wood and stone) non-ideal surfaces*, Colloid. Surface. A, 206 (1–3), 485–495.

Sakorafa V., Michailidis K., Burragato F., 1996, *Mineralogy, geochemistry and physical properties of fly ash from the Megalopolis lignite fields, Peloponnese, Southern Greece*, Fuel, 75 (4), 419–423.

Starov V. M., Kostvintsev S. R., Sobolev V. D., Velarde M. G., Zhdanov S. A., 2000, *Spreading of liquid drops over dry porous layers: complete wetting case*, J. Colloid Interf. Sci., 252 (2), 397–408.

Tavana H., Lam C. N. C., Grundke K., Friedel P., Kwok D. Y., Hair M. L., 2004, *Contact angle measurements with liquids consisting of bulky molecules*, J. Colloid Interf. Sci., 279 (2), 493–502.

Toscioglu C., Goodell B., Lopez-Anido R., Gardner D., 2004, *Surface energy characterization of preservative-treated wood and E-glass/phenolic composites*, Forest Prod. J., 54, 262–268.

Ulman A., 1991, *Ultrathin organic films*, Acad. Press, New York, 442 pp.

Van Oss C. J., Chaudhurry M. K., Good R. J., 1988, *Interfacial Lifshitz-van der Waals and polar interactions in macroscopic systems*, Chem. Rev., 88 (6), 927 –936.

Wenzel R. N., 1936, *Resistance of solid surfaces to wetting by water*, Ind. Eng. Chem., 28 (8), 988–994.